Process modeling for economic optimization of a solar driven sweeping gas membrane distillation desalination system

Sarah E. Moore[a], Sera Mirchandani[a], Vasiliki Karanikola[a], Tina M. Nenoff[b], Robert G. Arnold[a], A. Eduardo Sáez[a]

[a] Department of Chemical and Environmental Engineering, The University of Arizona, 1133 E. James E. Rogers Way, Harshbarger 108, Tucson, AZ 85721, United States
[b] Material, Physical, and Chemical Sciences Center, Sandia National Laboratories, P.O. Box 5800, MS 1514, Albuquerque, NM 87185, United States

Corresponding author: A.E. Sáez, esaez@email.arizona.edu, 1133 E. James E. Rogers Way, Harshbarger 108, Tucson AZ 85721, United States

Abstract

Water scarcity is especially impactful in remote and impoverished communities without access to centralized water treatment plants. In areas with access to a saline water source, point-of-use desalination by solar-driven membrane distillation (MD) is a possible method for mitigating water scarcity. To evaluate the applicability of MD, a comprehensive process model was developed and used to design an economically optimal system. Thermal energy for distillation was provided by solar thermal collectors, and electricity was provided using photovoltaic collectors. Distillation was performed using sweeping-gas membrane distillation. The cost of water in the optimized system was approximately $\$85/m^3$. Membrane modules and solar thermal collectors made up the largest portion of the cost. Neither thermal nor electrical energy storage was economical within current technologies. The model developed provides a template to optimize MD membrane characteristics specialized for point-of-use applications.

Graphical Abstract

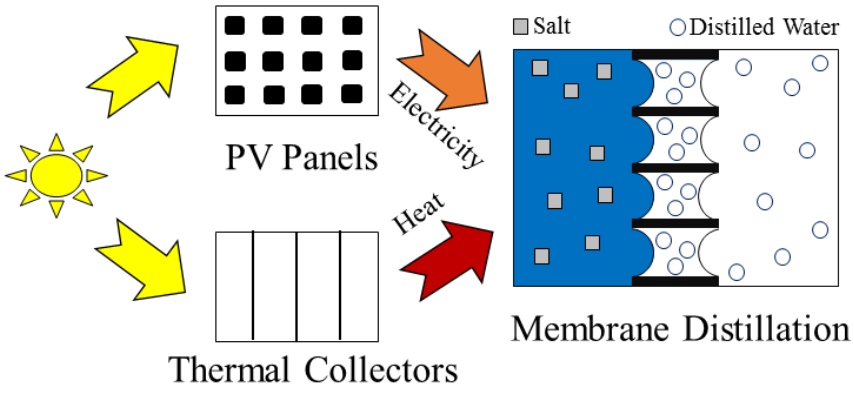

Keywords

Desalination; Solar energy; Membrane distillation; Optimization; Modeling

Highlights

- We present a model to compute the water cost from solar membrane distillation.
- Water produced using optimized solar membrane distillation costs \$85/m^3.
- Membranes and thermal collectors are the main contributors to capital cost.
- Analysis of the optimal system shows that energy storage is not economical.

1 Introduction

Over 2.7 billion people are impacted by water scarcity (Hoekstra et al., 2012). Population growth and climate change may increase that number to over five billion by 2025 (United Nations Department of Economic and Social Affairs, 2015). Many drought-stricken areas also have high poverty rates, which makes coping with water shortages especially challenging with far-reaching consequences. However, the possibility of access to seawater or brackish ground water makes desalination a feasible alternative for mitigating drought. Desalination is energy

intensive and therefore relatively expensive. A large fraction of impoverished communities is remote and not electrified; energy requirements must be met without access to a centralized power grid. Solar-driven desalination technologies may be appropriate for mitigating water scarcity under these circumstances. One example is membrane distillation (MD), a thermal process in which the energy required for desalination can be provided as solar thermal energy, rather than photovoltaic (PV) energy. Under some circumstances, this provides substantial cost savings over pressure-driven systems.

Khayet (2013) reviewed energy consumption and cost of MD systems. Reported unit energy consumption varied by three orders of magnitude, and costs varied by nearly four orders of magnitude (Figure 1). Previous studies also show that high operating temperatures improved energy efficiency (Khayet, 2011) (Khayet & Matsuura, 2011).

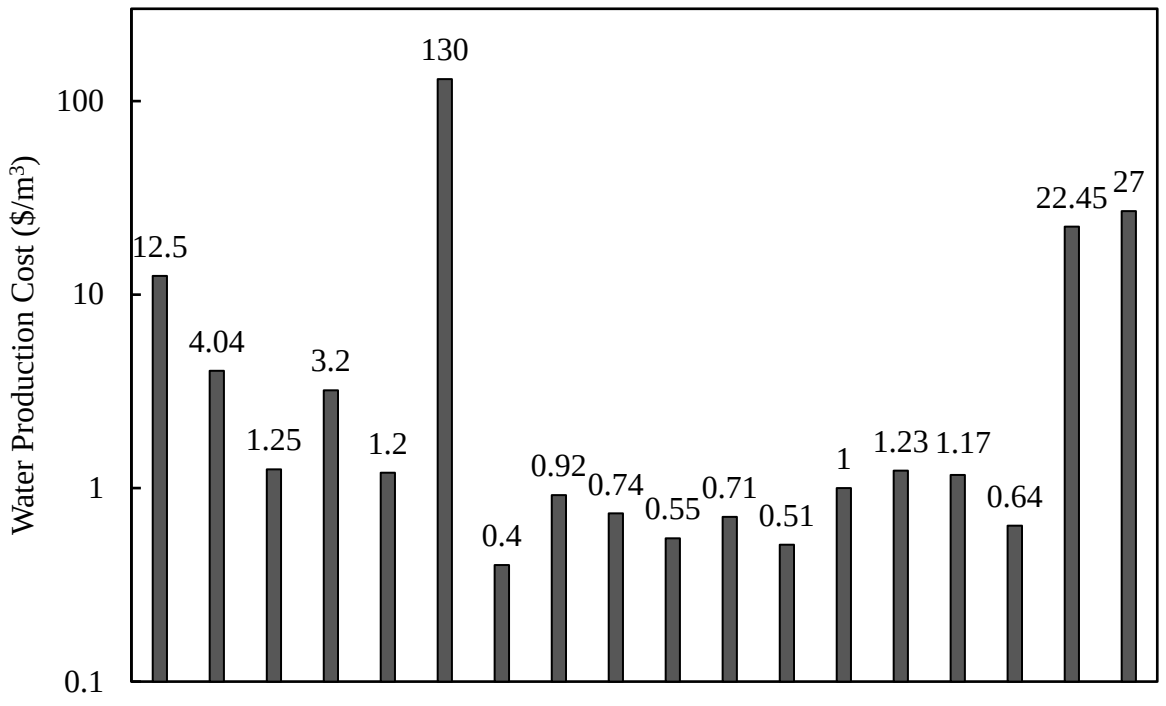

Figure 1. Reported membrane distillation water production costs. System configuration, energy source, and methods for cost calculation varied. Details are given in Khayet (2013). In this data set, water production varied from 0.017 m^3/day ($130/$m^3$) to 24,000 m^3/day ($1.17/m^3).

It is unclear from the cited studies whether high operating temperatures and improved energy efficiency reduce cost. Overall, however, enough is known about MD technology to suggest that it may provide adequate water production. Additional understanding is needed to anticipate cost savings that are likely to accrue from technology maturation, improved membrane design and selection, and system optimization.

To date, few researches have attempted to optimize MD system design. Chang et al. (2014) provided a cost estimate and optimization for air-gap MD. In that study, thermal energy was provided by solar thermal collectors and grid electricity was used to provide electrical power to the system. Membrane performance was modeled from first principles using Aspen Custom Modeler. The cost of water was calculated from a pseudo-steady process model and optimized using a quadratic programming algorithm. The decision variables were confined to area of the solar collectors and various flow rates. The cost of water from the optimized system varied from \$5.16-\$15.7/m^3 for systems with capacities varying from 100-1,000 kg of water produced per day. As expected, water produced from small capacity systems was more expensive. Optimization improved calculated costs relative to cost estimates performed without optimization. While the results demonstrated the benefit of system optimization, next generation modeling research is needed to address important factors not covered in past studies. These include the effects of using PV electricity instead of grid power and introducing energy storage components into the system, consideration of different MD operating modes, such as sweeping-gas MD (SGMD), and optimization of additional decision variables, including those related to equipment sizes and the times at which the system operates.

Here we present a detailed process model developed to predict the cost of water from a SGMD system. Water production rates are determined from first principles using a state-of-the-

art membrane model for hollow-fiber modules (Karanikola et al., 2015), and the cost of water was calculated using standardized methods (Khayet, 2013). An optimization algorithm was added to minimize the unit cost of water in economically optimal systems. The economically optimal system was used to evaluate the economic feasibility of SGMD and to make recommendations for future research. Results indicate that water produced from an optimal solar-driven SGMD designed to produce 240 L/day costs approximately $\$85/m^3$ and remains economically uncompetitive. The operation of the optimal system was analyzed to show that neither electrical nor thermal energy storage provide economic benefit. Further work is needed to develop economical energy storage devices and membranes specialized for MD in order to improve competitiveness of the technology for solar desalination.

2 Modeling Methods

2.1 Process Model and Optimization Overview

The SGMD process is modeled and optimized using methods discussed below and algorithms included in MATLAB 2016a. A schematic describing the process model and optimization is provided in Figure 2. The optimization algorithm selects decision variable values and sends them to the process model. Decision variables considered in this study, including various equipment sizes, flow rates, and operational parameters, are listed in Table 2. The process model calculates system design parameters and models one day of operation to calculate the process variables as a function of time and the water produced in a day. Next, the model calculates the amortized cost of water. If the cost of water is non-optimal, the optimization algorithm selects new decision variable values, and the process is repeated until the cost of water can no longer be reduced.

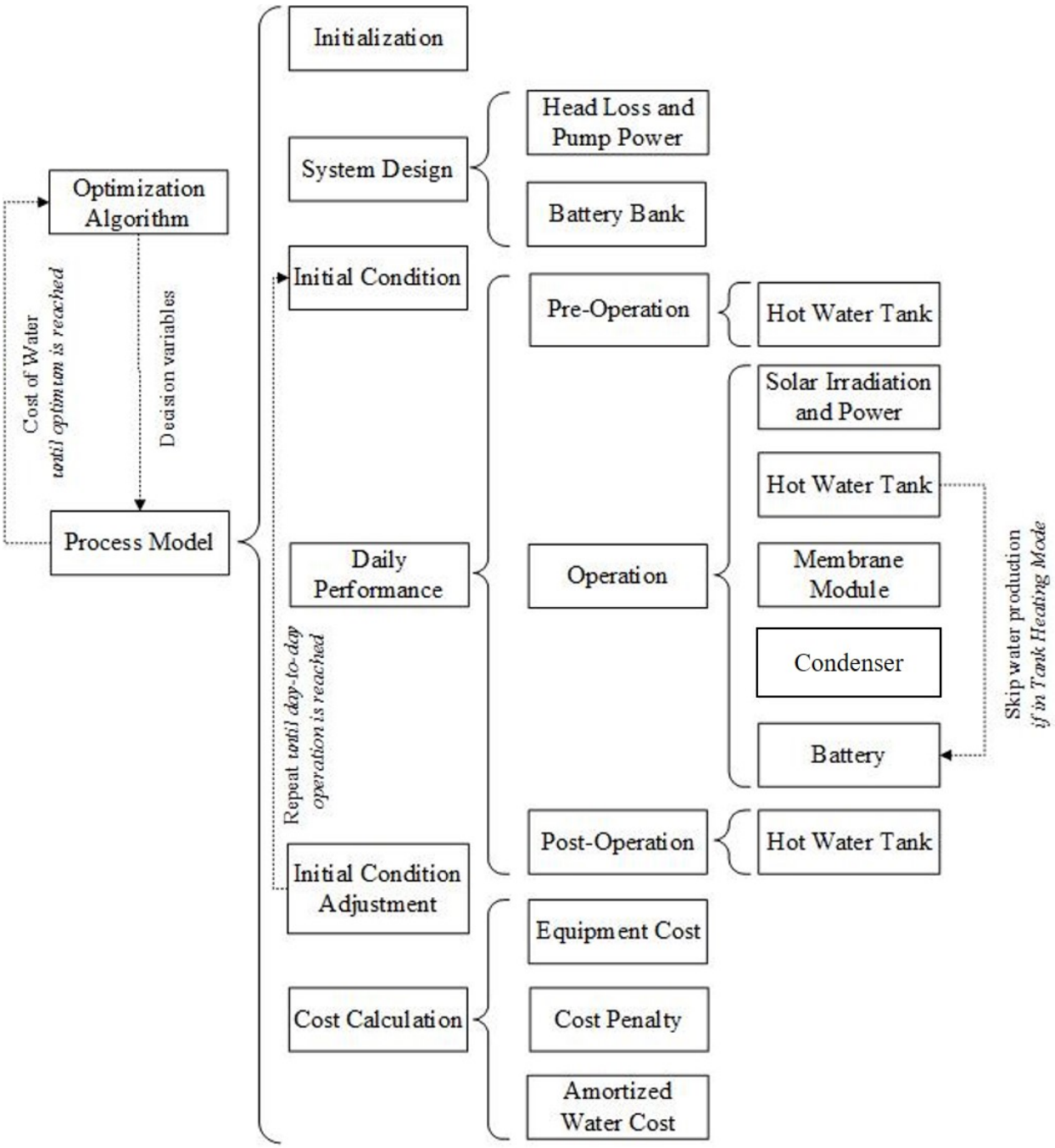

Figure 2. Optimization and process model schematic.

The SGMD system simulated is shown in Figure 3. Solar irradiation is collected by independent photovoltaic (PV) and thermal arrays. The PV collectors are used to power the pumps and blowers and charge the battery. When there is insufficient electric power from the PV collectors, the battery discharges to satisfy the power demand. The thermal collectors are used to heat the

heat exchange fluid, a 50% by volume mixture of propylene glycol and water, which is circulated through a heat exchanger in the hot water tank at a volumetric flow rate, Q_G, (stream 1, Figure 3) to heat the untreated water. The glycol solution is returned to the thermal collectors (stream 2) to complete the glycol loop. The heated water is fed into the lumen side of the membrane module (stream 4) at flow rate of Q_{HW}. After the module, the remaining brine is returned to the hot water tank (stream 5) to complete the hot water loop. Untreated make-up water (stream 3) is fed into the hot water tank at a flow rate equal to the permeate production rate to maintain a constant liquid volume. Ambient air is fed into the shell side of the membrane module (stream 8) at a flow rate of Q_{AIR}. The humid air stream leaving the membrane module (stream 7) is fed to a condenser. The air stream is cooled using an ambient cooling water stream, assumed to be taken from the same source as the untreated water, at a flow rate of Q_{CW} (stream 9). After the condenser, the cooling water stream is discarded (stream 6). Rejected air leaves the condenser in stream 10, and the condensed permeate is collected in stream 11. Condensate is

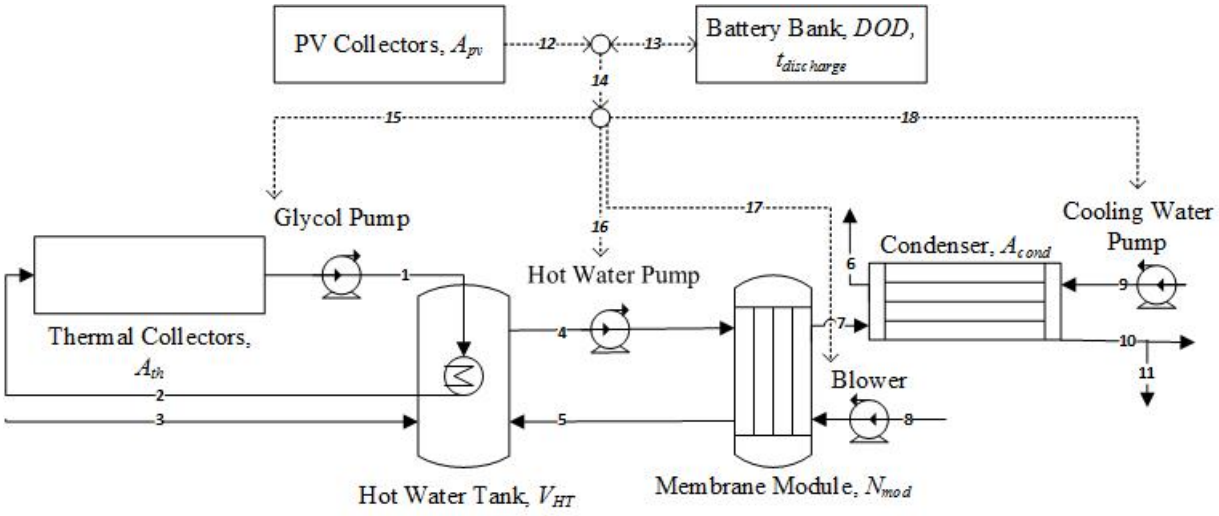

Figure 3. Solar SGMD System Schematic. Fluid flows are shown as solid lines and electrical energy transmission is indicated by dotted lines. Process decision variables are in italics. Fluid/energy transmission lines and variables shown are identified.

blended with untreated water to produce a potable blend. Here the ratio of untreated to treated water is assumed to be 2:1, selected to bring a typical brackish groundwater sample to 500 mg/L TDS, the secondary MCL for potable water (Barnhart et al., 2011).

A process model was developed to calculate the cost of water as a function of the decision variables and design constraints as shown in Figure 1. First, the process model is initialized, a step in which values of the decision variables, design constraints, and other constants are loaded into the program. Second, the system head loss, pump power, and battery bank size are calculated from decision variables, constraints, and constants set in the previous step. Third, initial conditions (e.g., fluid temperatures) are selected before the algorithm enters a loop in which system performance is modeled over one day of operation.

The daylong operating period simulated is broken down into three periods: pre-operation, operation, and post-operation: (1) Pre-operation runs from midnight to the start of the operating period; the start time is a decision variable; (2) operation runs from the beginning to the end of the operating period, also a decision variable; and (3) post-operation extends from the end of the operating period to midnight. During the pre- and post-operating periods, the system is not running and only environmental heat losses from the hot water tank are calculated.

The operating period is further broken down into two operational modes: tank heating mode and water production mode. In the tank heating mode, the glycol loop transports heat from the solar collectors into the hot water tank, but all other fluid loops are inactive and no water is produced. In the water production mode, the system is fully operational, and water is produced via membrane distillation. During water production, the solar irradiance, fluid temperatures, and water produced are calculated for each time step. The model operates identically during heating mode, although no water is produced. The times at which water production begins and ends are

decision variables; the system operates in heating mode between the start time and water production start time.

The aim is to simulate daylong operations, not startup. To achieve this, the conditions of process variables at the end of the day are compared to the initial conditions. If they do not match, the time loop runs again with the initial conditions set to the final conditions from the previous run. This process repeats until the initial and final conditions are essentially equal. Finally, the model calculates the equipment and operational costs, applies a penalty if the water production requirement is unmet, and calculates the amortized cost of water. Penalties were large enough to eliminate solutions that do not meet the water production constraint from consideration by the optimization algorithm. At this point, the process model returns the cost of water to the optimization algorithm, which selects new decision variables. This process is repeated until the optimization algorithm accepts the solution as optimal.

2.1.1 Initialization

During initialization, the values of decision variables, design constraints and constants are set. There are fourteen decision variables for which values must be provided by the user or optimization algorithm, shown in Table 2. The decision variables are the independent variables that drive the design, operation, and cost of the SGMD system.

Other constants and design parameters are loaded into the program. Parameters that affect system design and operation include location settings (altitude, latitude, longitude, and ambient temperature for the period of operation simulated), water production requirement (L/day), and feed water salinity (expressed as NaCl molarity). Since the model runs for a single day, the date selected for optimization must be representative of the period of interest from the perspective of design. Parameter values selected are summarized in the Supplementary Information (section

S7). Note that many values are site specific; results are sensitive to location, regional weather characteristics, and raw water characteristics.

2.2 System Design

After initialization, calculations are performed to size pumps and batteries as functions of specified design relationships and constraints. The performance relationships presented below are later used to simulate process operation (section 2.3) and calculate the cost of water (section 2.4).

2.2.1 Head Loss and Pump Power

The system head loss is calculated for the air, brine, cooling water, and glycol streams as a function of the decision variables using the Darcy-Weisbach equation (Neto, 2014). The power required to overcome the head losses and deliver the required flow rates is then determined. Detailed calculation procedures are provided in the Supplementary Information (section S1).

2.2.2 Battery Bank

After power requirements for pumping air, brine, cooling water, and glycol streams are calculated, the total system power requirement during the water production period, P_{demand}, is determined from equation (1).

$$P_{demand} = P_{hw_{pump}} + P_{a_{pump}} + P_{g_{pump}} + P_{cw_{pump}} \quad (1)$$

where $P_{hw_{pump}}$, $P_{a_{pump}}$, $P_{g_{pump}}$, and $P_{cw_{pump}}$ are the pump powers required to circulate the hot water, air, glycol, and cooling water, respectively. The battery system size is determined from the total power requirement. The amount of time that the system is to be powered by the batteries alone, $t_{discharge}$, is assumed to 15 hours. The value was selected so that the battery bank would be capable of producing water for one day in the case that power is not generated due to cloud cover

or other operational difficulties. The power requirement during water production, which is a constant, is assumed to represent operations throughout $t_{discharge}$. This ignores the possibility that results of the optimization may require the system to operate the glycol loop alone, heating the brine without water production. In that case, the power demand is equal to the glycol circulation power requirement alone. It is important to note that using the total power demand to size the battery system represents a conservative approach to battery design.

The battery capacity is a non-linear function of the discharge time in hours (equation 2). This relationship relates only to the discharge of 12 V lead-acid batteries. Equation (2) is developed using a least squares regression analysis to fit the manufacturer-provided data (Concorde Battery Corp., 2013). The average sustainable discharge current, *I*, is shown in equation (3).

$$E_{MAX} = 13.8 \ln\left(t_{discharge}\right) + 84.4,\ 1\text{ h} \leq t_{discharge} \leq 120\text{ h} \tag{2}$$

$$I = \frac{E_{MAX}}{t_{discharge}} \tag{3}$$

where $t_{discharge}$ is the discharge time in hours and E_{MAX} is the battery capacity in Ampere hours. Equation (2) fits the data in the range $1\text{ h} \leq t_{discharge} \leq 120\text{ h}$.

The average power each battery can provide, P_b, for the specified discharge time is given by equation (4).

$$P_b = IV \tag{4}$$

where *I* is the sustainable discharge current calculated in equation (3) and *V* is the battery voltage (Concorde Battery Corp., 2013).

For an ideal battery system in series configuration with no inefficiencies, the number of batteries necessary, $N_{b_{ideal}}$, is given by equation (5).

$$N_{b_{ideal}} = \frac{P_{demand}}{P_b} \quad (5)$$

Battery banks, however, have several factors that can decrease their energy storage capacity and the power that is delivered to the system. The depth of discharge (DOD) is the fraction of the total capacity utilized. There is an inverse relationship between expected battery life and the depth of discharge (described in section 2.3.5). The DOD is treated as a decision variable in the model presented here. The battery charging and discharging efficiency, η_{bcd}, also reduces useful battery capacity, as some energy is lost in charging and discharging the battery. Here the battery charging and discharging efficiency is set to 80% (Concorde Battery Corp., 2013). The overall relationship between the actual number of batteries required and the number required in a theoretical situation in which inefficiencies are absent is indicated in equation (6).

$$N_{b_{actual}} = \frac{N_{b\,ideal}}{DOD \cdot \eta_{bcd}} \quad (6)$$

Note that the usable battery capacity may be increased by increasing the battery discharge time or by increasing the depth of discharge. Usable battery capacity should be variable, and including either discharge time or DOD as decision variables would accomplish this. Testing of the process model indicated that the depth of discharge had a minor effect on the cost of water, but the discharge time had no effect at all. This is due to the fact that equation (2) is insensitive to the discharge time except for very short discharge times. Therefore, the depth of discharge was treated as a decision variable, and the discharge time was kept constant at a value of 15 hours to allow for approximately one day of water production without solar power.

2.3 Process Simulation

The operation portion of the process model simulates the physical performance of the system during each time step. Each quantity in the operational section is calculated once per time step.

This includes the solar irradiance and power, temperatures and flow rates of relevant streams, and the battery state of charge. The goal of the process simulation is to calculate the water produced during a day of operation. This value is compared to the water production requirement, and a penalty is applied if the production requirement is not satisfied.

2.3.1 Solar radiation and power

This first part of the operational model is the calculation of solar radiation available for the SGMD system. The solar radiation model is used to find the normal beam and diffuse radiation intensities in Watts per square meter at the location of the system, both of which can be converted into electrical and thermal energy. Next, the thermal power, P_{th}, and electrical power, P_{pv}, are determined as a function of the normal beam and diffuse radiations, and the solar thermal and PV collector geometries and areas. Methods adapted from Duffie and Beckman (2013) are detailed in the Supplementary Information (section S2).

2.3.2 Hot Water Tank

The temperature of the water in the hot water tank is calculated from an energy balance using a control volume that includes the hot water tank and the thermal collectors (equation 7).

$$\frac{dE}{dt} = \dot{E}_{TH} + \dot{E}_{HWi} + \dot{E}_{MW} - \dot{E}_{HWo} - \dot{E}_{ELHT} \tag{7}$$

When multiplied by the time increment, $\frac{dE}{dt}$ represents the accumulation of thermal energy in the control volume; $\dot{E}_{TH}$, $\dot{E}_{HWi}$, and $\dot{E}_{MW}$ are the energy inputs due to the the solar thermal collectors, the water entering the hot water tank from the modules, and the makeup water entering the hot water tank during the time step, respectively, during the same time interval; and $\dot{E}_{HWo}$ and $\dot{E}_{ELHT}$ are the energy outputs due to the water leaving the hot water tank and environmental losses from control volume.

Equation (7) simplifies to equation (8) based on the following assumptions: (i) The tank is well mixed so that the temperature of water in the tank is equal to the temperature of water leaving the tank, and (ii) environmental losses from areas in the control volume other than the hot water tank can be neglected.

$$\rho_w V_{HT} c_{pw} \frac{dT_{HWo}}{dt} = \tag{8}$$

$$P_{th} + c_{pw} Q_{HWi} T_{HWi} + c_{pw} Q_{MW} T_{MW} - c_{pw} Q_{HWo} T_{HWo}$$

$$- U_{tank} A_{tank} (T_{HWo} - T_{amb})$$

Here, ρ_w is the density of liquid water; V_{HT} is the volume of water in the hot water tank; c_{pw} is the specific heat capacity of liquid water; T_{HWo} is the temperature of the hot water leaving the tank; P_{th} remains the rate at which thermal energy is provided by the solar thermal collectors, as calculated by equation (S24) of the Supplementary Information; Q_{HWi}, Q_{HWo}, and Q_{MW} are the volumetric flow rates of hot water entering and leaving the hot water tank and make-up water entering the tank, respectively; T_{HWi}, T_{HWo}, T_{MW}, and T_{amb} are the temperatures of the hot water entering and exiting the tank, the make-up water, and the ambient air; U_{tank} is the overall coefficient for heat transfer between the water in the hot water tank and the surrounding environment; and A_{tank} is the surface area of the hot water tank available for heat transfer to the environment. U_{tank} and A_{tank} are calculated from manufacturer-provided information, as detailed in the Supplementary Information (section S3).

The time derivative of T_{HWo} is estimated using a forward-difference first order formula, equation (9). Equation (9) is substituted into equation (8) and solved for $T_{HWo}(t + \Delta t)$ (equation 10). A time step of one minute is used in this study.

$$\frac{dT_{HWo}}{dt} \approx \frac{T_{HWo}(t + \Delta t) - T_{HWo}(t)}{\Delta t} \tag{9}$$

$$T_{HWo}(t+\Delta t) = \tag{10}$$

$$T_{HWo}(t) + \frac{\Delta t}{\rho_w V_{HT} c_{pw}}\{P_{th}(t) + c_{pw}Q_{HWi}(t)T_{HWi}(t) + c_{pw}Q_{MW}(t)T_{MW}(t)$$

$$- c_{pw}Q_{HWo}T_{HWo}(t) - U_{tank}A_{tank}(T_{HWo}(t) - T_{amb})\}$$

In order to maintain a constant volume in the tank, the flow rate of make-up water must be equal to the permeate flow rate, $Q_P(t)$. A mass balance on the membrane module shows that the return flow of brine to the hot water tank is equal to the flow of hot water from the tank minus the permeate produced, or $Q_{HWi}(t) = Q_{HWo} - Q_P(t)$. Finally, it is assumed that the makeup water enters the tank at ambient temperature. Substitution into equation (10) yields equation (11).

$$T_{HWo}(t+\Delta t) = \tag{11}$$

$$T_{HWo}(t) + \frac{\Delta t}{\rho_w V_{HT} c_{pw}}\{P_{th}(t) + c_{pw}[Q_{HWo} - Q_P(t)]T_{HWi}(t) + c_{pw}Q_P(t)T_{amb}$$

$$- c_{pw}Q_{HWo}T_{HWo}(t) - U_{tank}A_{tank}(T_{HWo}(t) - T_{amb})\}$$

The permeate flow rate, $Q_P(t)$, and $T_{HWi}(t)$ are calculated in the membrane model for time t, as described in section 2.3.3.

A temperature control system was added to the hot water tank model. This control system prevents the water in the tank from heating to above 90 ºC, since higher temperatures will damage the membrane. If the temperature exceeds 90 ºC during any time step, the program restores the 90 ºC value. This simplification neglects the effects that the control system may have on the rest of the process, including, for example, power required to adjust control elements in the system to maintain the temperature below the set point.

If the water production period selected is shorter than the system's operating period, water is not produced during a fraction of the operating period. The hot water tank temperature is then calculated from equation (11), setting the permeate flow rate to zero and the temperature of water returned to the tank (T_{HWi}) equal to the temperature in the tank (T_{HWo}).

During the system operation period, as selected by the optimization algorithm, the hot water tank temperature is calculated as a function of time from equation (11). Outside the operating period, the system is off, no water is produced and glycol is not circulated to transfer heat from the thermal collectors to the tank. Under these conditions, the only term remaining in the tank energy balance is the heat loss to the environment (equation 12).

$$T_{HWo}(t+\Delta t) = T_{HWo}(t) - \frac{\Delta t}{\rho_w V_{HT} c_{pw}}\{U_{tank} A_{tank}(T_{HWo}(t) - T_{amb})\} \qquad (12)$$

2.3.3 Membrane Module

The water production rate, temperature of the air-water gas stream, and the temperature of the brine returning to the hot water tank are calculated using a hollow-fiber membrane distillation (HFMD) model developed previously (Karanikola et al., 2015). Inputs to the HFMD model include the temperature of the inlet hot water, hot water flow rate, and air flow rate entering the membrane module. The model calculates the temperature of the exit air, temperature of the hot water, and permeate flow rate leaving the membrane module. The HFMD model is based on detailed energy and mass balances in discretized sections of the hollow fiber module. The model accounts for thermal convection on the brine and permeate sides of the membrane, diffusion/conduction through the membrane, and convective mass transfer on the permeate side. This predictive model was validated against experimental data obtained using a variety of commercial membranes

Module cost	$1500
Membrane area	1.03 m^2
Module length	12.7 cm
Module diameter	6.35 cm
Porosity	0.25
Tortuosity	7
Number of fibers	6454
Fiber outer diameter	400 µm
Fiber inner diameter	300 µm
Pore diameter	0.03 µm

Table 1. Characteristics of membrane module used in process simulation (Membrana, 3M, 2013)

(Karanikola et al., 2015) (Karanikola et al., 2017). The characteristics of the membranes used in this work are listed in Table 1.

2.3.4 Condenser

The condenser model calculates the amount of liquid water that is condensed from the gas stream exiting the membrane module. It is assumed that the air exiting the condenser is saturated with water and that environmental heat losses are negligible. Due to the relatively small scale of the application, a plate-and-frame condenser is taken as the basis for the model.

Four equations based on mass and energy balances, provided in the Supplementary Information (section S4), are solved for the temperature of the cooling water exiting the condenser (T_{CWo}), the heat duty (q), the mass flow rate of water condensed ($\dot{m}_{WC}$), and the temperature of the air leaving the condenser (T_{AIRo}). Condensate accumulated over the daily water production period is the daily water production.

2.3.5 Battery

When the available PV power exceeds system power requirements, excess power charges the batteries until they are at full capacity. Conversely, when available power is less than power demand, the batteries discharge to meet the power requirement until they reach their maximum depth of discharge (DOD). In this way, battery operation is governed by the state of charge

(SOC), defined as the charge stored in the battery divided by the battery capacity. SOC is calculated using equation (13) (Tazvinga et al., 2015).

$$SOC(t+\Delta t) = SOC(t) - \frac{\eta_{BCD}\Delta t}{E_{MAX} \cdot V}\left(P_{demand}(t) - P_{PV}(t)\right) \quad (13)$$

where η_{BCD} is the battery charge/discharge efficiency, E_{MAX} is the battery capacity, V is the battery voltage, P_{demand} is the power demand of the system, and P_{PV} is the power generated by the photovoltaic panels, as determined in section S2 of the Supplementary Information. The power demand depends on the operation mode and related decision variables at time *t*. If the system is in heating mode, the power demand is equal to the power required to run the glycol pump. When the system is in water production mode, the power demand is equal to the power required to run all four pumps. No power is required when the system is in off mode.

When the batteries are fully charged, the calculated $SOC(t+\Delta t)$ may exceed 1.0 if the excess power entering the battery results in a full charge at some point during Δt. If so, the model will reset SOC to 1.0. If the calculated $SOC(t+\Delta t)$ falls below the minimum charge allowed by the DOD, battery capacity has been exhausted, and the SOC is reset to its minimum value (1 – DOD), system operation is halted, and water production ceases.

It is important to consider the trade-offs associated with battery use. Running the battery allows the system to produce water when power demand exceeds PV power availability, but additional costs are associated with discharging the battery due to accompanying reductions to its lifetime. Battery lifetime in years is related to the battery use using the Ah-throughput method (Tazvinga et al., 2015), in which lifetime is quantified by considering the charge that passes in and out of a battery (throughput). In the Ah-throughput method, the battery lifetime is calculated by dividing the total throughput over its lifetime by the throughput over one year. The total lifetime throughput is the maximum usable capacity over one cycle of charging and discharging

($2DODE_{MAX}$) times the number of cycles that may be run before replacement. The annual throughput is calculated by integrating the charge in and out of the battery over one day of operation and multiplying by the number of days in a year. The result is given by equation (14).

$$Lifetime = \frac{2DODE_{MAX}C_{Fail}}{365\sum_{day}\frac{|P_{demand}(t) - P_{PV}(t)|}{V}\Delta t} \quad (14)$$

where C_{Fail} is the number of cycles to battery failure - a cycle is defined as charging and discharging the battery completely one time. The number of cycles to failure may be calculated as a function of DOD from manufacturer specifications, as in equation (15) (Concorde Battery Corp., 2013).

$$C_{Fail} = \begin{cases} -17{,}647DOD + 6764.7, 0.1 \leq DOD < 0.3 \\ -4125DOD + 2980, 0.3 \leq DOD < 0.5 \\ -1111DOD + 1411.1, 0.5 \leq DOD < 1 \end{cases} \quad (15)$$

Note that the Ah-throughput method used to determine equation (14) calculates the usable throughput available over the battery's lifetime (given in the numerator of equation (14)). This method does not consider the fact that operation at low state of charge shortens battery life further; this effect is neglected in this analysis, as are effects associated with temperature and other environmental conditions that may be detrimental to battery life.

2.3.6 Initial Condition Adjustment

At the start of the program, fluid temperatures are set equal to the ambient temperature, and the battery is at its maximum state of charge (SOC=1). At the end of the first time loop (i.e. simulation for a full 24 hours), the final values of the fluid temperature and state of charge are compared to the initial condition. If the sum of absolute percent differences for these two variables exceeds an arbitrary tolerance, the time loop runs again with the initial conditions set equal to the values at the end of the previous day. This process is repeated until the initial and

final conditions of each variable are essentially equal. Cost calculations can then be undertaken. This initial condition adjustment ensures that the optimization is carried out for a system with constant day-to-day operation instead of a system that is operating during a transition period.

2.4 Economic Calculations

2.4.1 Equipment Cost Calculation

Functions relating equipment costs to scale were developed from manufacturers' data for the pumps, blowers, hot water tank, condensers, and solar arrays. Cost functions are given in the Supplementary Information (section S5). Unit costs of off-the-shelf components such as membrane modules and batteries were taken as constant from manufacturers' data (Membrana, 3M, 2013) (Concorde Battery Corp., 2013). The total cost of each component was calculated by multiplying the unit cost by the number of units (modules, etc.) used in the design.

The model estimates equipment fittings and installation costs as 25% of the major equipment cost (Khayet, 2013). The model also includes miscellaneous costs for piping, additional storage tanks, air filters, and control systems. These costs are assumed to be independent of decision variable values and were calculated from a solar-driven sweeping gas membrane distillation pilot system constructed in the Navajo Nation (Barnhart et al., 2011). While the systems are similar in operation and capacity, they are different in several ways. Notably, the system described by Barnhart et al. (2011) generated solar power using a concentrated cogeneration system in which PV and thermal energy are generated simultaneously. Additionally, the system was not designed and operated under optimal conditions.

2.4.2 Cost Penalty

An important aspect of the process optimization is the need to satisfy the target water demand. The optimization problem presented here is rather complex due to the relatively large number of decision variables; under those circumstances, specification of a water demand constraint makes difficult the convergence of optimization algorithms. For this reason, we have included this constraint as a cost penalty (equation 16). The coefficient in the penalty cost function (1,000) is sufficiently strict to eliminate solutions that do not meet the water demand requirement. The production goal and actual production are given in liters per day.

$$Penalty\ (\$) = 1{,}000(Production\ Goal - Actual\ Production)^2 \qquad (16)$$

2.4.3 Amortized Water Cost

The objective function to be minimized during system optimization is the cost per liter of water that must be charged so that the net present value of the system is equal to zero at the end of the system lifetime. It was calculated using methods adapted from Seider et al. (2009) and Khayet (2013), including calculation of membrane and battery replacement, labor, and other operational costs. The system lifetime was taken as 20 years, and the interest rate as 5%. Additional parameters used and assumptions made are detailed in the Supplementary Information (section S6).

2.5 Optimization

The SGMD process is modeled as described in section 2.1-2.4 and optimized using algorithms available in MATLAB 2016a (see below). The amortized water cost, calculated by the process model, is minimized using several non-linear optimization algorithms available in MATLAB. The objective of the optimization is to find values for decision variables that produce the lowest

unit cost for water while satisfying the production constraint. The following procedure is used in the application of each optimization technique:

1. Enter initial values for each decision variable.
2. Run global optimization algorithm, detailed below.
3. Change initial values of each decision variable to the optimized values found in step 2.
4. Repeat steps 2 and 3 until the decision variable values selected by the optimization algorithm equal the input values.

Note that the optimization algorithm is restricted in the range of decision variables values from which it can select. That is, the user must provide a range of acceptable values for each decision variable, as well as an initial guess. Additionally, the optimization algorithm is confined to selection of decision variables values from a set of whole numbers in order to prevent selection of a nonphysical value (such as non-integer values for membrane modules) or from values that differ by a defined increment to guarantee a finite number of possible solutions. This ensures that the algorithm terminates. Values provided to the optimization algorithm, as well as their method of selection, are given in the Supplementary Information (section S7).

The optimization algorithms tested in this work include four available in MATLAB: (i) genetic, (ii) particle swarm, (iii) pattern search, and (iv) simulated annealing algorithms (MathWorks, 2016). Each algorithm selects values of decision variables to test using a specified method and calculates the objective function value as a function of the decision variables. It compares the objective function value to previous calculations in order to determine if an optimum has been reached. If the objective function value is not optimized, it selects new decision variable values to test. This continues until the algorithm arrives at the optimal solution (further manipulation of the decision variables cannot reduce the objective function value). The

methods differ in the route taken to decision variable optima. For example, the particle swarm algorithm selects decision variable values to test in a method inspired by the social swarming behavior of birds and insects (Kennedy & Eberhart, 1995).

Results from each algorithm were compared in terms of computational time required to identify an optimum and the quality of the optimum. Calculations showed that the particle swarm algorithm was the best on both counts, and it was subsequently used for all simulations. All MATLAB code used in this study is available from the MathWorks file exchange depository.

2.6 Decision Variable Partial Derivative Analysis

Further analysis was carried out to determine the sensitivity of the amortized cost to variation in each of the decision variables in the optimized system. Normalized partial derivatives are calculated using both forward and backward difference methods in order to evaluate the behavior of the objective functions on both sides of the optimum. The was done by varying the optimum value of each decision variable by a certain percentage in either direction (equations 17 and 18).

$$\frac{\partial c}{\partial\left(\frac{x}{x_{opt}}\right)}_{Forward} = \frac{c\left(x_{opt}+\Delta x\right)-c\left(x_{opt}\right)}{\Delta x}x_{opt} \tag{17}$$

$$\frac{\partial c}{\partial\left(\frac{x}{x_{opt}}\right)}_{Backward} = \frac{c\left(x_{opt}\right)-c\left(x_{opt}-\Delta x\right)}{\Delta x}x_{opt} \tag{18}$$

Here, *c* is the amortized water cost calculated using the objective function, and *x* represents each decision variable. x_{opt} is the decision variable value at the optimum, and Δx was selected to be 5% of the optimal decision variable value. The addition or subtraction of Δx often results in a decision variable value that fails to meet the water production requirement. The costs calculated for such solutions include a penalty, as described in section 2.4.2, resulting in an artificially high cost. As these solutions are infeasible, they were not included in the partial derivative analysis.

3 Results and Discussion

3.1 Optimization Results

An optimization was performed using the following design constraints:

- Potable water production requirement: 240 L/day
- Location: Leupp, Navajo Nation, Arizona, USA
- Day: March 20th
- Feed water salinity: 0 M

Note that the feed water salinity was set to 0 M so that the contribution of the salinity to the vapor pressure of water could be neglected. The price of water to recover capital and O&M costs for an optimally designed SMD system designed to produce 240 L/day of a potable blend is approximately \$84.7/m^3 over a twenty-year lifetime. Values of each decision variable in the optimally designed and operated system are presented in Table 2.

Cost of Water	\$84.7/m^3
Thermal collector area, A_{th}	27 m^2
Photovoltaic collector area, A_{pv}	4 m^2
Hot water tank volume, V_{HT}	100 L
Hot water flow rate, Q_{HW}	2.7 L/min
Air flow rate, Q_{AIR}	140 L/min
Cooling water flow rate, Q_{CW}	50 L/min
Glycol flow rate, Q_G	10 L/min
Number of membrane modules, N_{mod}	5 modules
Battery depth of discharge, DOD	0.65
Condenser area, A_{cond}	0.3 m^2
System start time, t_{start}	6:00 AM
System end time, t_{end}	4:10 PM
Water production start time, $t_{start_{water}}$	7:00 AM
Water production end time, $t_{end_{water}}$	4:10 PM

Table 2. Optimized cost of water and decision variables for the system specified above

The capital cost of the optimally designed SGMD system is approximately \$35,000. The contribution of each major piece of equipment is shown in Figure 4. Yard piping and related

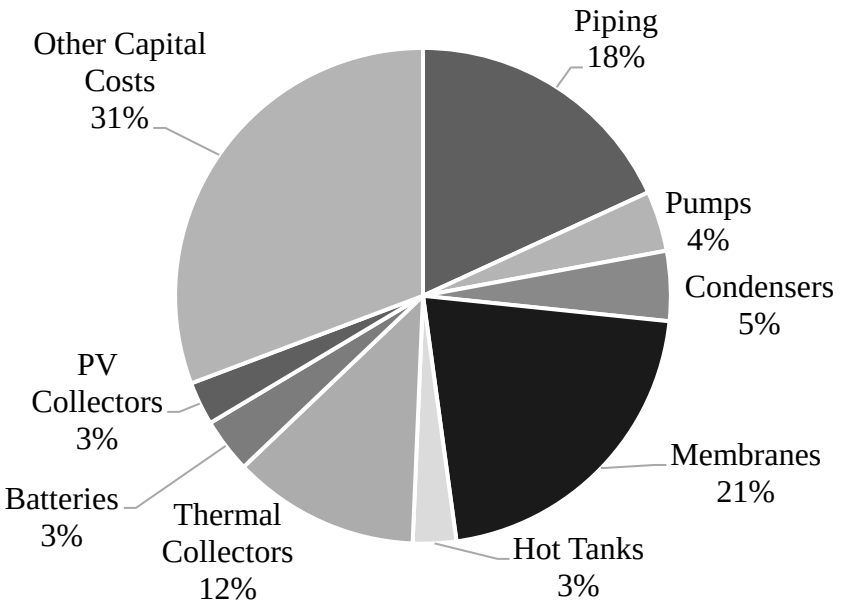

Figure 4. Capital cost breakdown for the optimized SMD system. The total capital cost was $35,400. Other capital costs include fees associated with site preparation, system start up, and contingencies.

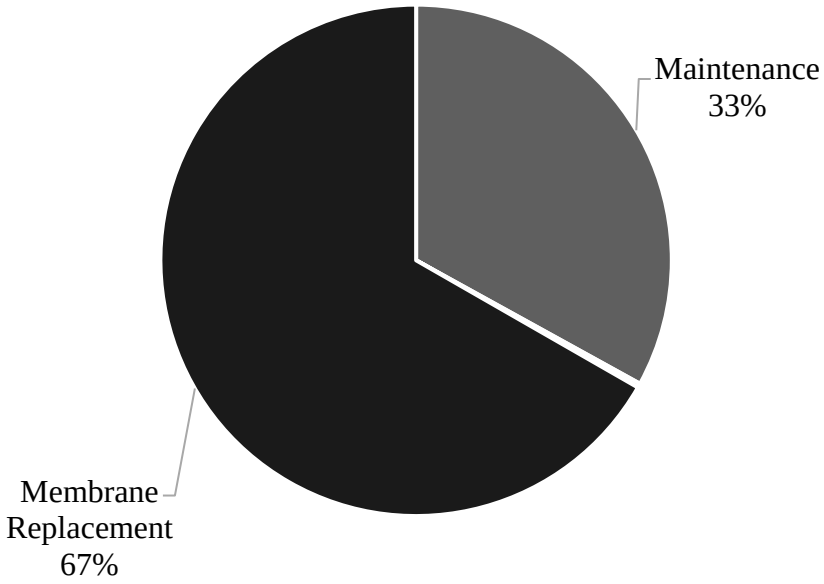

Figure 5. Average annual operating cost breakdown for the optimized SMD system. The operating cost averages $1,700 per year. Maintenance expenses include costs associated with routine replacement of fittings and minor equipment. The cost of labor for maintenance and brine disposal was also included in this calculation, but made up a negligible fraction of the operating expenses.

capital costs such as site preparation and contractor's fees make up almost half of the total capital cost. The membrane modules and thermal collectors make up the biggest fractions of major equipment costs.

The annual operating cost of the optimally designed system averages approximately $1,700 per year. As shown in Figure 5, he largest fraction of the operating cost (67%) goes to replacement of the membrane modules (assumed to have a lifetime of 5 years, in line with the manufacturer's recommendation). Maintenance costs make up the remaining 33% of the operating cost and include expenses associated with routine replacement of fittings and minor pieces of equipment, such as pumps. Costs associated with labor and brine disposal are also included in the operating expenses, but are negligible. Additionally, battery replacement is included in the calculation of the operating cost. However, the batteries are used so little in the optimal design that their lifetime exceeds the lifetime of the plant.

3.2 Operation of Optimal System

The process model is used to simulate the operation of the optimal system throughout a single, representative day of operation. Figure 6 shows the normal beam and diffuse solar irradiation as a function of time throughout the day. After sunrise (6:15 am), both the normal beam and diffuse radiation increase until noon and then decrease until sunset (5:30 pm). The normal beam irradiation is approximately an order of magnitude higher than the diffuse irradiation.

Figure 7 shows the power produced by both the thermal and the PV solar collectors as function of time on the day modeled. The thermal collectors produce about an order of magnitude more energy than the PV collectors due to greater area and higher efficiency. This is

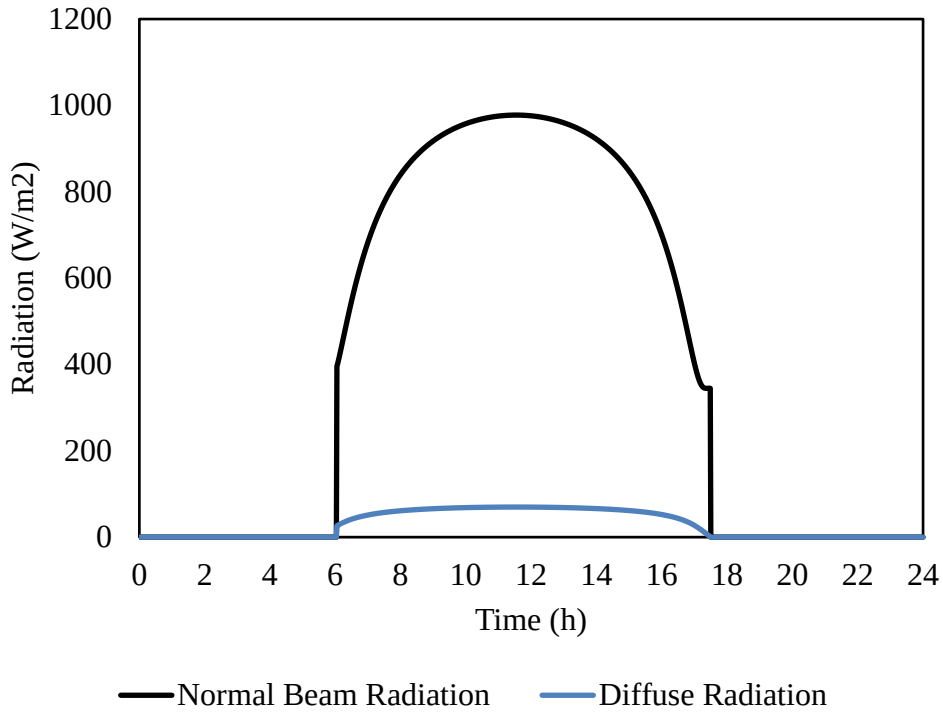

Figure 6. Clear sky ground level solar irradiation as a function of time for one day of operation (March 20 in Leupp, AZ). Time = 0 hours represents 12 am, while T = 24 hours represents 12 am of the following day.

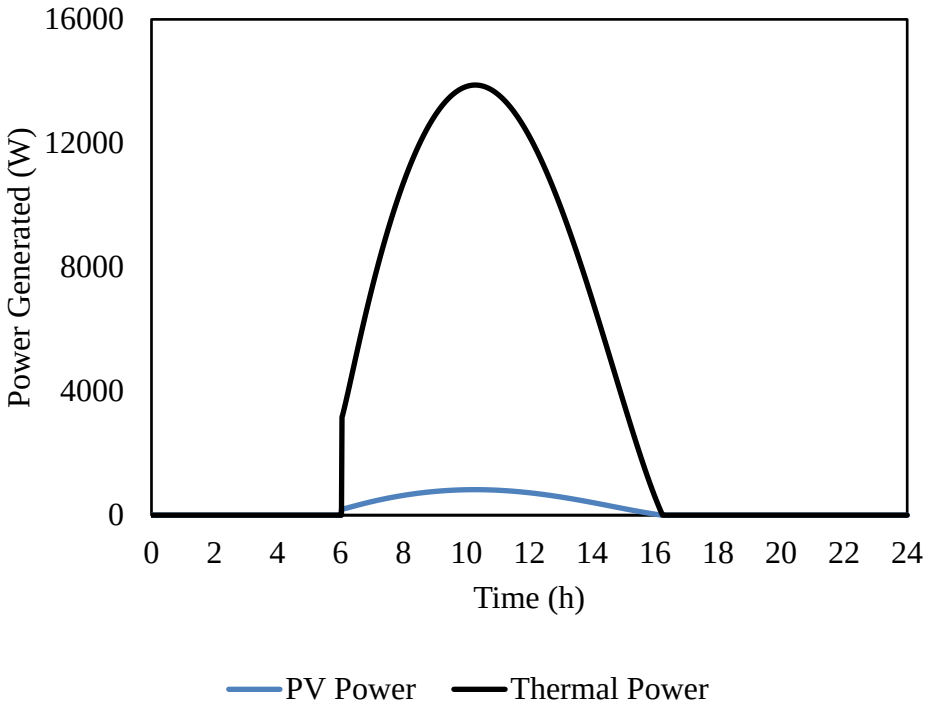

Figure 7. Thermal and electrical power generated as a function of time during one day of operation (March 20 in Leupp, AZ). Time = 0 hours represents 12 am, while T = 24 hours represents 12 am of the following day.

to be expected because most of the energy required for membrane distillation is used to provide the latent heat of water evaporation. Note that power produced by the collectors reaches zero before sunset. This is because the collectors are angled away from the setting sun.

Figure 8 illustrates the relationship between the electric power generated, power demand, and battery SOC throughout the day. During daylight hours, the power generated increases from sunrise until noon and decreases from noon until sunset.

After sunrise at approximately 6:00 AM, the glycol loop turns on and operates only the glycol pump, allowing the hot water tank to heat up. During that time, the system power demand is 0.26 W. At 7:00 AM, shortly after sunrise, water production begins and continues until sunset. During this period, the power demand is 606 W. The power demand is zero outside of the operating period selected by the optimization algorithm. When the power demand exceeds the power requirement, the battery discharges to satisfy demand. Conversely, when the power generated exceeds the demand, the battery charges. Note that the battery supplements PV power to produce water from about 1 PM to 4:10 PM; the system never operates off battery power alone.

Note that the battery never discharges completely. In fact, the battery is over 96% charged at the end of the operating period selected via optimization. While the DOD selected by the optimization algorithm was 0.65, the battery never discharges to its minimum allowable charge so the functional DOD is 0.04. This is somewhat counterintuitive, as there is substantial electrical energy remaining in the batteries that could be used to operate the system during the night and produce more water. However, the results of the optimization algorithm indicate that reduction of battery life due to additional use costs more than the value of incremental water

produced at the optimized unit cost. It can be concluded from this analysis that electrical energy storage provides limited net economic benefit in the solar-driven SGMD context.

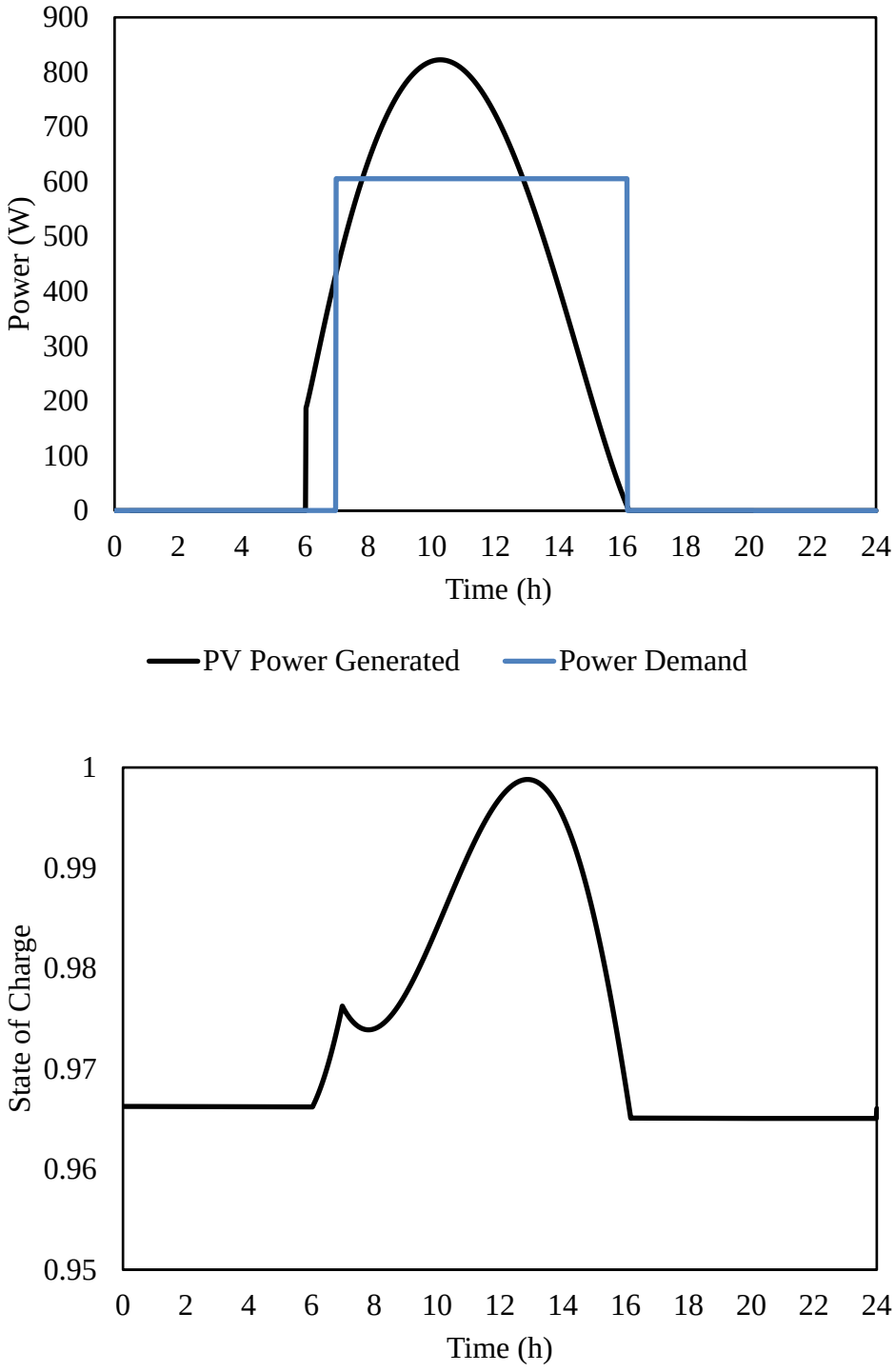

Figure 8 (top). Electrical power generation and demand as a function of time for one day of operation in the optimized SMD system.

Figure 8 (bottom). Battery state of charge as a function of time for one day of operation in the optimized SMD system. Note that the state of charge increases when the power generated exceeds the power demand and decreases when the power demand is greater than the power generated until the battery reaches it minimum charge (1-DOD). Time = 0 hours represents 12 am, while T = 24 hours represents 12 am of the following day.

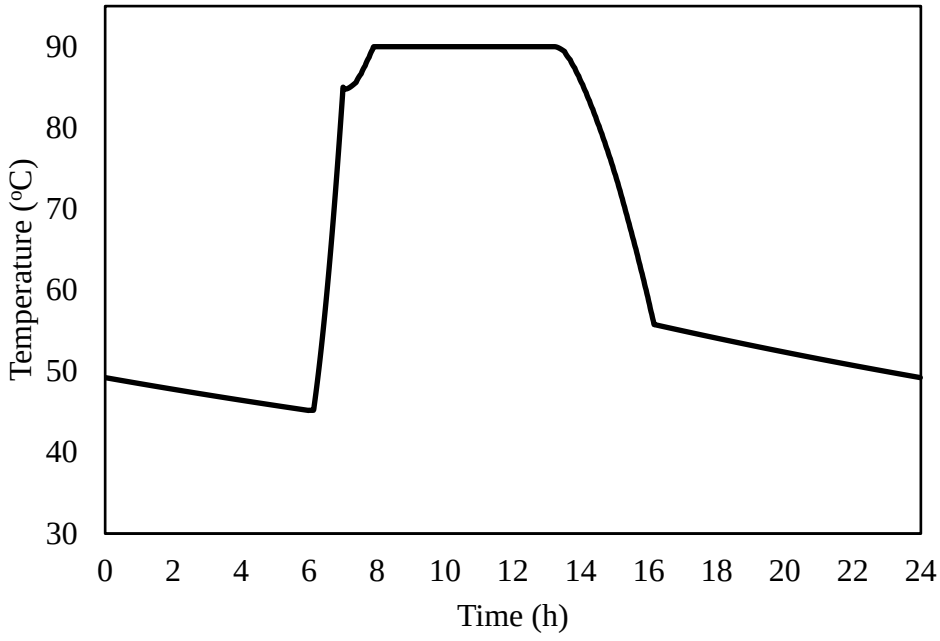

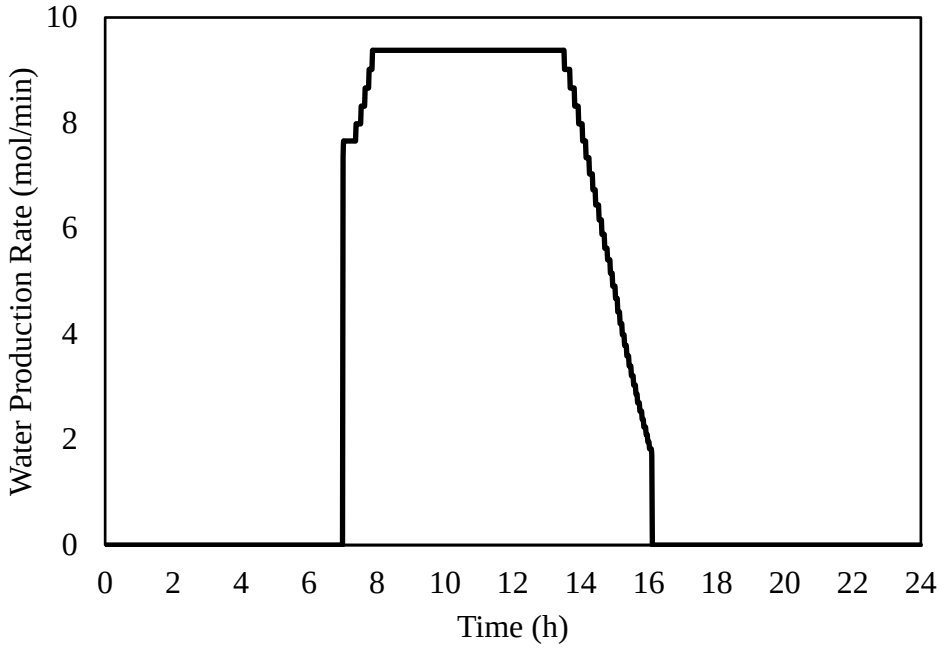

Figure 9 (top). Hot water tank temperature as a function of time for one day of operation in the optimal SMD system. Figure 9 (bottom). Water production rate as a function of time for one day of operation in the optimal SMD system. Time = 0 hours represents 12 am, while T = 24 hours represents 12 am of the following day.

Figure 9 illustrates the temperature in the hot water tank and water production rate throughout the day in the optimized system. At midnight, the system is off and no water is produced. From there, the temperature in the hot water tank decreases slowly due to environmental losses. Immediately after sunrise, there is sufficient PV power available to begin circulating the glycol loop in order to transfer heat into the hot water tank.

After sunrise (6:00 AM), water temperature in the hot water tank increases to about 80 ºC before water production is initiated. Thereafter, the hot water tank continues to heat up, but at a slower rate since the heat of water evaporation must be provided. At about 8:00 AM, the hot water tank temperature stabilizes at 90 ºC due to the temperature control system. After about 2 pm, the temperature begins to decrease and continues to do so until the end of the operating period. The operating period ends at 4:10 PM, after which the hot water tank temperature decreases more slowly, again due to environmental losses alone. As expected, the water production rate is a strong function of the temperature in the hot water tank.

It is interesting to note that the system reaches its maximum temperature and maximum water production rate early in the day, at approximately 8:00 AM. After this time, additional thermal energy collected cannot go to increasing the temperature in the hot water tank without exceeding temperature limits of the MD membrane; it must go towards replacing the heat lost to evaporation of water. Thus, at least part of the available thermal heat is wasted. During the period of operation at the maximum temperature, the heat of evaporation of water accounts for approximately 70% of the thermal energy collected. The remaining 30% is unusable. One could hypothesize that wasting heat is not economical and should be reduced. This can be accomplished by reducing the thermal collector area. Doing so would also lead to a reduced capital cost. However, a lower thermal collector area would also lead to a longer startup time,

and thus a shorter period of operation at the maximum temperature and water production rate. In other words, there is a trade-off associated with the thermal collector area: a large collector area leads to larger average water production rates at higher thermal collector cost, while a small collector area reduces capital cost and wasted heat, but has lower average rate of production. The optimization algorithm selected a relatively large collector area, indicating that an increase in capital cost is balanced by the increase in the time operating at the maximum temperature. Similar arguments surround the number of membrane modules selected. That is, wasted thermal energy could be minimized by increasing the number of membrane modules. This would be sub-optimal, however, since the increase membrane costs would apparently outweigh benefits derived from a higher water production rate, shorter operating time and less waste thermal energy.

This is similar to the findings of other studies, which conclude that high operating temperature leads to improved energy efficiency in MD systems (Khayet, 2011). This analysis provides some evidence that improvements in efficiency may lead to cost improvements. However, the cost-optimal system presented here is highly inefficient, as much of the thermal energy produced cannot be used. Future studies could be used to optimize first- and second-law efficiency in order to further investigate the relationship between cost and efficiency for solar desalination systems.

The optimally designed system includes a 100 L hot water tank, which is the smallest allowed volume. A small hot water tank costs relatively little and heats up quickly at the start of system operation, supporting more hours of daily operation at the maximum water production rate. However, a small tank will also cool quickly at night, lowering the number of evening hours during which the system remains operational. To expose these relationships, the unit cost

of water and volume of water produced by the SMD system are calculated for three different hot water tank sizes: 100 L, the optimal size, 1,000 L, and 10,000 L, the largest allowable size. Results are summarized in Table 3. Calculations are performed with all other decision variables constant at their optima.

Hot Water Tank Volume (L)	Cost of Water ($/m^3)	Water Produced (L/day)
100	84.7	240
1,000	118	231
10,000	452	96

Table 3. Cost of water and water production for three different hot water tank sizes

Figure 10 shows the hot water tank temperature and water production rates for the three different hot water tank sizes as functions of time. Not surprisingly, the 1,000 L hot water tank reaches the maximum allowable temperature of 90 ^{o}C, and thus its maximum water production rate, after the smaller hot water tank. While it maintains its temperature longer, it fails to produce enough water to meet the water production requirement due to its slow startup. There is no economic benefit to the higher cost associated with a larger tank, so the amortized cost of water is higher than for the optimal hot tank size. This effect is especially evident for the largest hot water tank size, which never reaches the maximum temperature or water production rate. Little water is produced to pay back the cost associated with a very large tank, so the cost of water is high.

The largest hot water tank can be made more economical by (1) increasing the thermal collector area in order to increase the temperature in the hot water tank, (2) extending the operating window, and (3) further discharging the battery so that the system operates into the night. However, the results of the optimization indicate that the increase in capital cost associated with a larger hot water tank and thermal collector area and the increase in operating

costs associated with a longer operating period outweigh the economic benefits associated with heat storage. It must be concluded that thermal energy storage is economically infeasible, much

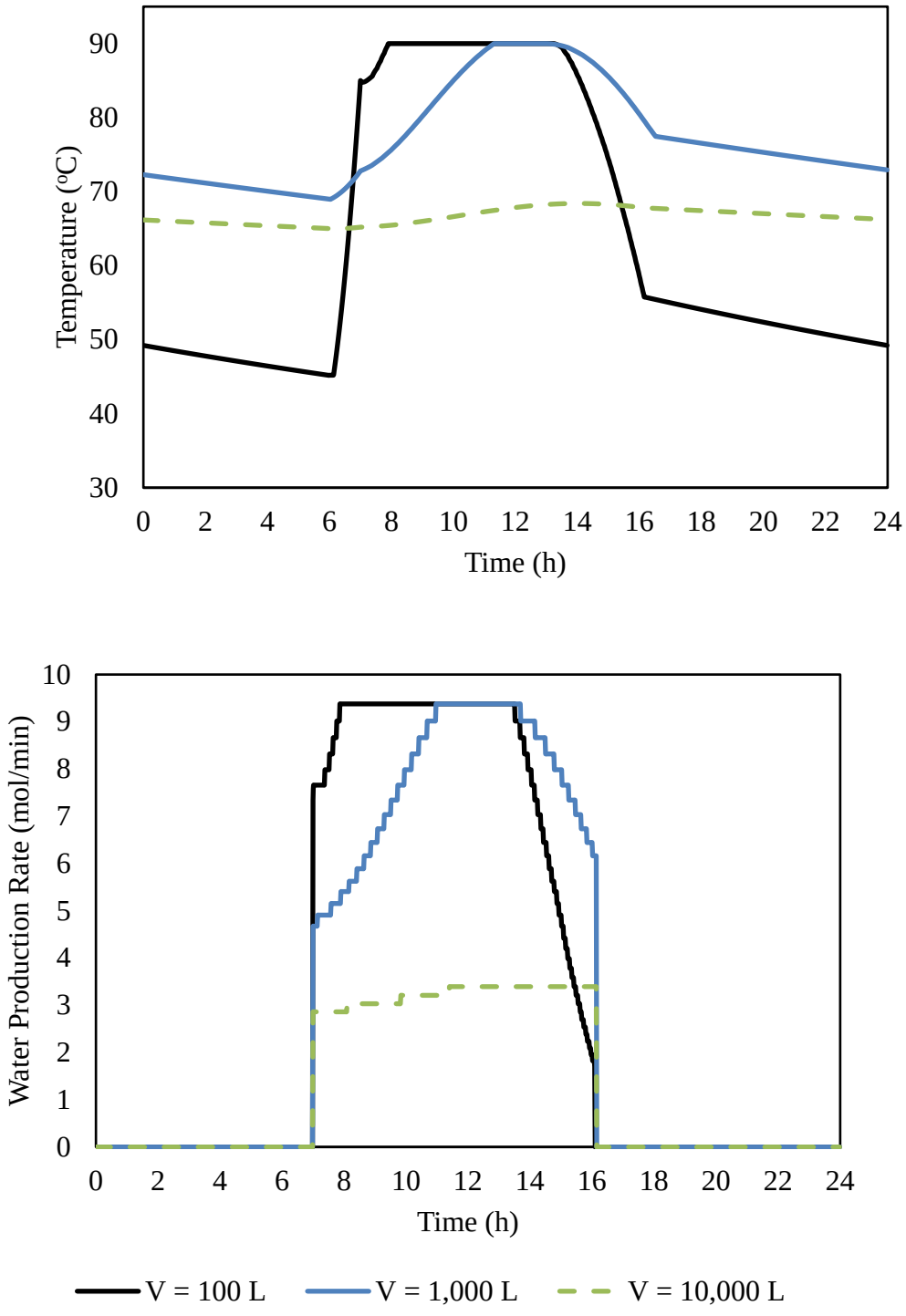

Figure 10 (top). Hot water tank temperature as a function of time for one day of operation using three different hot water tank sizes.

Figure 10 (bottom). Water production rate as a function of time for one day of operation using three different hot water tank sizes.

like electrical energy storage. Previous studies have come to similar conclusions for both thermal (Gude et al., 2012) and electrical energy storage in solar desalination (Mohamed et al., 2008) (Qiblawey et al., 2009). Future studies might consider replacing the hot water tank with a direct heat exchanger to determine if any amount of energy storage is economically justified.

3.3 Decision Variable Partial Derivative Analysis

The importance of each decision variable to the cost of water is evaluated by estimating the normalized partial derivative of the amortized water cost near the global optimum with respect to each decision variable. First, normalized partial derivatives are estimated using a forward difference method, as in equation (17). Results are shown in Figure 11. As expected, all partial derivatives are greater than or equal to zero. This indicates that the cost of water increases as the decision variable value increases above the optimum value, supporting the idea that the identified optima represent a true optimum.

For a few decision variables, an incremental increase in the variable value resulted in a design that failed to meet the water production requirement. These variables include the air flow rate and the water production start and end time. Of the remaining decision variables, the number of membrane modules and thermal collector area have the largest partial derivatives, indicating that they have an important effect on the cost of water when increased relative to their optimum values. This result is intuitive, as the modules and thermal collectors make up the largest fraction of the equipment cost, as shown in Figure 4.

In order to evaluate the behavior of the objective function when decision variables are decreased individually, normalized partial derivatives are estimated using a reverse difference method, as in equation (18). It should be noted that all partial derivatives are less than or equal

to zero. This indicates that the cost of water increases as the decision variable value decreases away from its optimum, evidence that the solution identified by the optimization algorithm is a true optimum. However, an incremental decrease in nearly all the decision variables results in failure to satisfy the water production constraint and are omitted here as trivial.

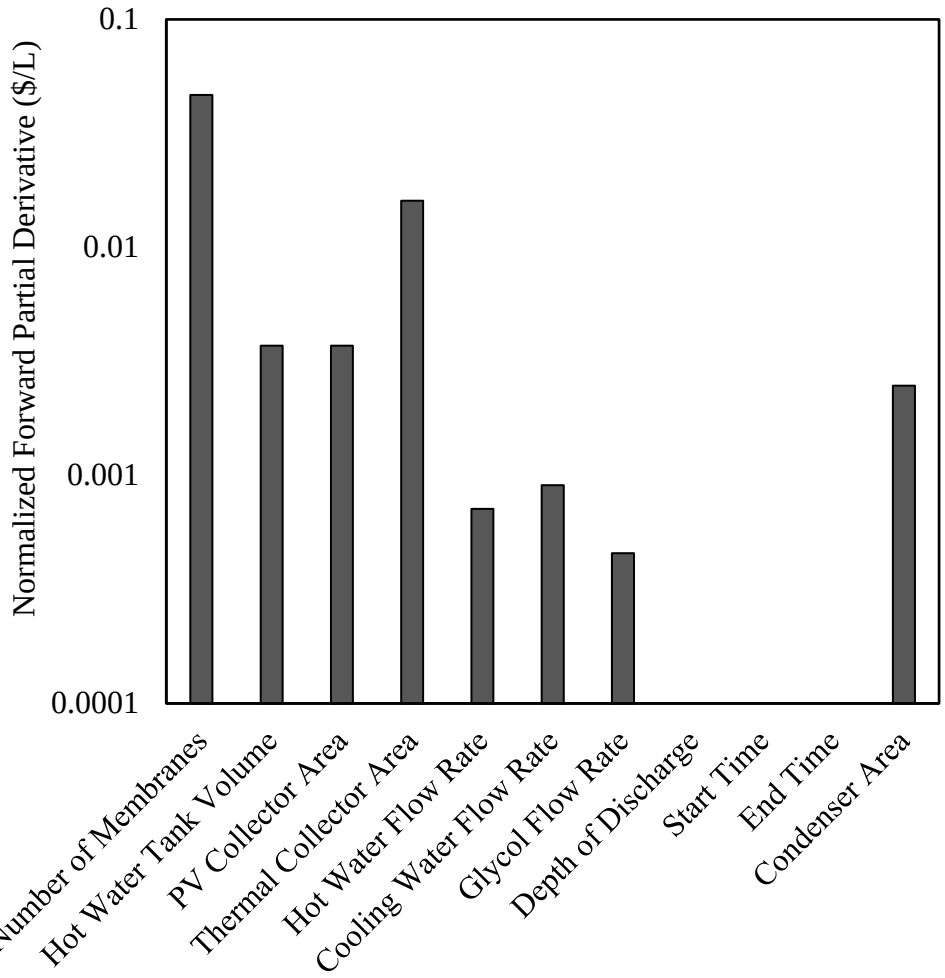

Figure 11. Normalized forward partial derivatives of the amortized cost of water near the optimum with respect to each decision variable.

5 Conclusions and Recommendations

5.1 Conclusions

A non-steady process model is developed to simulate a sweeping gas membrane distillation system powered by solar thermal and photovoltaic power for the desalination of drinking water.

The cost of water is estimated from manufacturer-provided equipment costs and various economic heuristics. Multi-variable optimization is performed in MATLAB to minimize the cost of water. The unit cost of water in the optimized system for cost recovery over a 20-year service life is $84.7 per cubic meter, which is higher than costs of water available from alternative sources. The total capital cost is $35,000, about half of which was for equipment. The membrane modules and thermal collectors comprise the biggest fraction of the equipment cost. The average annual operating cost is about $1,700 per year. Membrane replacement costs are the largest fraction of operating cost. Additionally, partial derivatives of the total present value cost with respect to each decision variable indicate that the number of membrane modules and thermal collector area have the largest effect on the amortized cost of water. This, combined with the fact that they make up the largest fraction of the equipment cost, indicate that future work in membrane distillation should be focused on improving the economics of these processes.

The optimized cost reported here exceeds most previously reported costs (Chang et al., 2014) (Khayet 2013). Other studies neglect important cost considerations, such as miscellaneous capital expenses or the cost of electricity. In a few places, equipment costs used here may already exceed those of available alternatives. For example, the hollow fiber membranes selected here cost $1,500/m^2, whereas the flat-sheet membranes used in (Chang et al., 2014) cost approximately $410/m^2. While the use of flat sheet membranes may provide cost savings, they cannot be implemented in a compact installation as is required for small scale systems. Further work is needed to model and optimize the use of compact membranes specialized for membrane distillation.

The hot water tank selected is the smallest permitted by the algorithm, indicating that the thermal energy storage associated with a larger hot water tank is uneconomical, and the overall

design may be improved by further limiting hot water storage. Several other decision variables, including the photovoltaic collector area, flow rates, and operating period configuration, are selected to minimize battery use, suggesting that neither thermal nor electrical energy storage leads to economy in solar-driven SGMD water purification. Although the solution is specific to geographic conditions (latitude, longitude and raw water quality) at Leupp, AZ, using March 20 as a representative day, this solution and accompanying analysis provides general guidance related to the cost of water purification via SGMD and the sensitivity of those costs to equipment-related and operational decision variables. The same or similar methods can be used for solar-driven SGMD system optimization in any geographic location.

5.2 Recommendations

The model and methods presented can be used to estimate the effects of design constraints and the impact of geographic variables on the cost of water purification by solar SGMD. Major equipment costs inform recommendations regarding improvements necessary to make this technology economically competitive. Additional work is necessary to illustrate the effect of the water production constraint (economies of scale) and location on optimization results. Additionally, results are expected to be highly sensitive to the day selected for modeling of daily water production due to variations in solar irradiation and weather. Future models should consider annual operation to account for the effect of this constraint.

The model can be used to optimize membrane characteristics such as pore size, tortuosity, and module dimensions rather than to optimize the SGMD system design as presented here. This will help inform the development of membranes specialized for membrane distillation. Next steps include extending this methodology to system optimization for spiral wound membrane modules as opposed to hollow fiber membranes of a single type. Spiral wound

membrane modules have been associated with higher permeate fluxes and show promise for improving energy efficiency and cost of membrane distillation (Winter et al., 2011) (Winter et al., 2017).

Acknowledgements

The authors would like to acknowledge the Campus Executive Laboratory-Driven Research and Development program at Sandia National Laboratories for their financial support of this work, and Jim Miller, Mike Hightower, Scott Paap, Brandon Heimer, Patrick Mette, and Wendell Ela for recommended model improvements and other helpful discussions.

Sandia National Laboratories is a multimission laboratory managed and operated by National Technology and Engineering Solutions of Sandia, LLC., a wholly owned subsidiary of Honeywell International, Inc., for the U.S. Department of Energy's National Nuclear Security Administration under contract DE-NA-0003525.

A.1 Nomenclature

Variable	Description	Units
A_{cond}	Condenser heat exchange area	m^2
A_{pv}	Photovoltaic collector area	m^2
A_{tank}	Hot water tank surface area	m^2
A_{th}	Thermal solar collector area	m^2
c	Amortized cost of water	$/$m^3$
C_{Fail}	Battery cycles to failure	cycles
c_{pw}	Heat capacity of water	J/(kg-K)
DOD	Depth of discharge	(none)

E	Energy contained in control volume	J
$\dot{E}_{ELHT}$	Rate of environmental losses through hot tank	W
$\dot{E}_{HWi}$	Rate of energy entering hot tank through hot water entering tank	W
$\dot{E}_{HWo}$	Rate of energy leaving hot tank through hot water exiting tank	W
E_{MAX}	Maximum battery bank capacity	A-h
$\dot{E}_{MW}$	Rate of energy entering hot tank through makeup water entering tank	W
$\dot{E}_{TH}$	Rate of thermal energy entering hot tank	W
I	Average battery current	A
$\dot{m}_{WC}$	Mass flow rate of water condensed in condenser	kg/s
$N_{b_{actual}}$	Actual number of batteries	(none)
$N_{b_{ideal}}$	Ideal number of batteries	(none)
N_{mod}	Number of Membrane Modules	(none)
$P_{a_{pump}}$	Air pump (blower) power	W
P_b	Battery power	W
$P_{cw_{pump}}$	Cooling water pump power	W
P_{demand}	Total power demand	W
$P_{g_{pump}}$	Glycol pump power	W
$P_{hw_{pump}}$	Hot water pump power	W
P_{pv}	Power produced by PV collectors	W
P_{th}	Power produced by solar thermal collectors	W

q	Condenser heat duty	J
Q_{AIR}	Air flow rate through a single MD module	L/min
Q_{CW}	Cold water flow rate	L/min
Q_G	Glycol flow rate	L/min
Q_{HW}	Hot water flow rate through a single MD module	L/min
Q_{HWi}	Flow rate of water entering the hot tank (leaving module)	L/min
Q_{HWo}	Flow rate of water leaving the hot tank (entering module)	L/min
Q_{MW}	Make up water flow rate	L/min
Q_P	Permeate flow rate	L/min
SOC	Battery state of charge	(none)
t	Time	min
T_{AIRo}	Temperature of sweeping gas leaving condenser	^oC
T_{amb}	Ambient temperature	^oC
T_{CWo}	Temperature of cooling water exiting condenser	^oC
$t_{discharge}$	Battery discharge time	h
t_{end}	System end time	min
$t_{end_{water}}$	Water production end time	min
T_{HWi}	Temperature of hot water entering hot tank (leaving module)	^oC
T_{HWo}	Temperature of hot water leaving hot tank (entering module)	^oC
T_{MW}	Temperature of make-up water	^oC
t_{start}	System start time	min
$t_{start_{water}}$	Water production start time	min

U_{tank}	Hot water tank overall heat transfer coefficient	W/(m^2-^{o}C)
V	System voltage	V
V_{HT}	Volume of hot water tank	L
x	Decision variable value	(varies)
x_{opt}	Optimal decision variable value	(varies)
Δt	Time step	min
Δx	Decision variable incremental change	(varies)
η_{bcd}	Battery charge/discharge efficiency	(none)
ρ_w	Density of water	g/mL

References

Barnhart, A., Ela, W., & Frisvold, G. (2011). Navajo Nation Solar Desalination Researh Pilot Demonstration Project.

Chang, H., Chang, C.-L., Hung, C.-Y., Cheng, T.-W., & Ho, C.-D. (2014). Optimization study of small-scale solar membrane distillation desalination systems. *International Journal of Environmental Research and Public Health, 11*, 12064-12087. doi:http://dx.doi.org/10.3390/ijerph111112064

Concorde Battery Corp. (2013). *Sun Xtender PVX-1290T Solar Battery Specifications*. Retrieved 2016, from http://www.sunxtender.com/solarbattery.php?id=36

Duffie, J., & Beckman, W. (2013). *Solar Engineering and Thermal Processes, 4th Edition.* Madison, WI, USA: Wiley. doi:http://dx.doi.org/10.1002/9781118671603

Gude, V., Nirmalakhandan, N., Deng, S., & Maganti, A. (2012). Low temperature desalination using solar collectors augmented by thermal energy storage. *Applied Energy,* 466-74. doi:http://dx.doi.org/10.1016/j.apenergy.2011.10.018

Hoekstra, A. Y., Mekonnen, M. M., Chapagain, A. K., Mathews, R. E., & Richter, B. D. (2012). Global Monthly Water Scarcity: Blue Water Footprints versus Blue Water Availability. *Plos One, 7*(2). doi:http://dx.doi.org/10.1371/journal.pone.0032688

Karanikola, V., Corral, A. F., Jiang, H., Saez, A. E., Ela, W. P., & Arnold, R. G. (2015, Feb 7). Sweeping Gas Membrane Distillation: Numerical Simulation of Mass and Heat Transfer in a Hollow Fiber Membrane Module. *Journal of Membrane Science, 483*, 15-24. doi:http://dx.doi.org/10.1016/j.memsci.2015.02.010

Karanikola, V., Corral, A. F., Jiang, H., Saez, A. E., Ela, W. P., & Arnold, R. G. (2017). Effects of membrane structure and operational variables on membrane disitllation performance. *Journal of Membrane Science*, 87-96. doi:http://dx.doi.org/10.1016/j.memsci.2016.11.038

Kennedy, J., & Eberhart, R. (1995). Particle Swarm Optimization. *Proceedings of IEEE International Conference on Nerual Networks* (pp. 1942-1948). IEEE. doi:http://dx.doi.org/10.1109/ICNN.1995.488968

Khayet, M. (2011). Membranes and theoretical modeling of membrane distillation: a review. *Advanced Colloid Interface Science*, 56-88. doi:http://dx.doi.org/10.1016/j.cis.2010.09.005

Khayet, M. (2013). Solar desalination by membrane distillation: Dispersion in energy consumption analysis and water production costs (a review). *Desalination, 308*, 89-101. doi:http://dx.doi.org/10.1016/j.desal.2012.07.010

Khayet, M., & Matsuura, T. (2011). *Membane Distillation: Principles and Applications.* Amsterdam: Elsevier. doi:http://dx.doi.org/10.1016/B978-0-444-53126-1.10020-X

MathWorks. (2016). *Global Optimization Toolbox Functions*. Retrieved 2016, from MathWorks Documentation: http://www.mathworks.com/help/gads/functionlist.html

Membrana, 3M. (2013, Sept 9). *Liqui-Cel Membrane Contactors: 2.5x8 Extra-Flow Product Data Sheet*. Retrieved 2016, from http://www.liquicel.com/uploads/documents/2%205x8ExtraFlow-D59Rev16%2010-15%20_ke.pdf

Mohamed, E., Papadakis, G., Mathioulakis, E., & Belessiotis, V. (2008). A direct coupled photovoltaic seawater reverse osmosis desalination system toward battery based systems -- a technical and economic experimental comparative study. *Desalination*, 17-22. doi:http://dx.doi.org/10.1016/j.desal.2007.01.065

Neto, O. (2014, Sep). Method for determining friction head loss along elastic pipes. *Irrigation Science, 32*(5), 329-339.

Qiblawey, H., Banat, F., & Al-Nasser, Q. (2009). Laboratory setup for water purification using household PV-driven reverse osmosis unit. *Desalination Water Treatment*, 53-9. doi:http://dx.doi.org/10.5004/dwt.2009.695

Seider, W. D., Seader, J. D., Lewin, D. R., & Widagdo, S. (2009). *Product and Process Design Principles: Synthesis, Analysis, and Evaluation.* John Wiley & Sons, Inc.

Tazvinga, H., Zhu, B., & Xia, X. (2015). Optimzal power flow management for distributed energy resources with batteris. *Energy Conservation and Management, 102*, 104-110. doi:http://dx.doi.org/10.1016/j.enconman.2015.01.015

United Nations Department of Economic and Social Affairs. (2015). *Water Scarcity*. Retrieved 2016, from Internation Decade for Action 'Water for Life': http://www.un.org/waterforlifedecade/scarcity.shtml

Winter, D., Koschikowski, J., & Wieghaus, M. (2011). Desalination using membrane distillaiton: Experimental studies on full scale spiral wound modules. *Journal of Membrane Science*, 104-112. doi:http://dx.doi.org/10.1016/j.memsci.2011.03.030

Winter, D., Koschikowski, J., Gross, F., Maucher, D., Duver, D., Jositz, M., . . . Hagedorn, A. (2017). Comparative Analysis of Full-Scale Membrane Distillation Contactors - Methods and Modules. *Journal of Membrane Science*, 758-771. doi:http://dx.doi.org/10.1016/j.memsci.2016.11.080